Combining Unique Planar Biaxial Testing with Full-Field Thickness and Displacement Measurement for Spatial Characterization of Soft Tissues

Daniel Pearce,[1] Mark Nemcek,[1] and Colleen Witzenburg[1,2]

[1]Department of Biomedical Engineering, University of Wisconsin-Madison, Madison, Wisconsin
[2]Corresponding author: *witzenburg@wisc.edu*

Published in the Neuroscience section

Soft tissues rely on the incredible complexity of their microstructure for proper function. Local variations in material properties arise as tissues develop and adapt, often in response to changes in loading. A barrier to investigating the heterogeneous nature of soft tissues is the difficulty of developing experimental protocols and analysis tools that can accurately capture spatial variations in mechanical behavior. In this article, we detail protocols enabling mechanical characterizations of anisotropic, heterogeneous soft tissues or tissue analogs. We present a series of mechanical tests designed to maximize inhomogeneous strain fields and in-plane shear forces. A customized, 3D-printable gripping system reduces tissue handling and enhances shear. High-resolution imaging and laser micrometry capture full-field displacement and thickness, respectively. As the equipment necessary to conduct these protocols is commercially available, the experimental methods presented offer an accessible route toward addressing heterogeneity. © 2022 The Authors. Current Protocols published by Wiley Periodicals LLC.

Basic Protocol 1: Unique biaxial testing of soft tissues and tissue analogs
Basic Protocol 2: Full-field thickness measurement of soft tissues and tissue analogs
Support Protocol 1: Creating and speckling cruciform-shaped samples for mechanical testing
Support Protocol 2: Creating custom gripping system to minimize sample handling

Keywords: anisotropy • biomechanics • digital image correlation • heterogeneity • inverse mechanics • laser micrometry

How to cite this article:
Pearce, D., Nemcek, M., & Witzenburg, C. (2022). Combining unique planar biaxial testing with full-field thickness and displacement measurement for spatial characterization of soft tissues. *Current Protocols*, *2,* e493. doi: 10.1002/cpz1.493

INTRODUCTION

Quantifying the mechanical behavior of soft biological tissues produces valuable information that can be linked to the structural constituents of the tissue, creating a more

Current Protocols e493, Volume 2
Published in Wiley Online Library (wileyonlinelibrary.com).
doi: 10.1002/cpz1.493
© 2022 The Authors. Current Protocols published by Wiley Periodicals LLC. This is an open access article under the terms of the Creative Commons Attribution-NonCommercial-NoDerivs License, which permits use and distribution in any medium, provided the original work is properly cited, the use is non-commercial and no modifications or adaptations are made.

26911299, 2022, 7, Downloaded from https://currentprotocols.onlinelibrary.wiley.com/doi/10.1002/cpz1.493 by University of Wisconsin,Madison Cam Department of Pathology and, Wiley Online Library on [19/12/2022]. See the Terms and Conditions (https://onlinelibrary.wiley.com/terms-and-conditions) on Wiley Online Library for rules of use; OA articles are governed by the applicable Creative Commons License

holistic picture of how they behave and adapt to mechanical loading. Early polymer scientists demonstrated the utility of biaxial tests for mechanically characterizing thin, highly deformable materials (Rivlin, 1948; Rivlin & Saunders, 1951; Treloar, 1948). The theory and methods in these fundamental studies were further developed by biomechanists for soft tissues, which often function as highly deformable membranes in the human body (Lanir & Fung, 1974a, 1974b). Since it was popularized in the mid-20th century, implementation of biaxial testing has often relied on the assumption of homogeneous strain fields and negligible in-plane shear forces (Sacks, 2000). These assumptions are appropriate for isotropic, homogeneous materials; however, soft biological tissues typically exhibit pronounced anisotropy and heterogeneity. Additionally, shear is often a physiologically relevant loading mechanism for soft tissues due to the structure of their complex fibrous extracellular matrix (Claeson & Barocas, 2017; Gardiner & Weiss, 2001; Sacks, 1999). Thus, the inclusion of shear in mechanical tests may result in more reliable and physiologically relevant material constant approximations.

In this article, we present protocols for unique biaxial testing and full-field thickness measurement for the mechanical characterization of soft biological tissues and tissue analogs. These samples commonly undergo large, complex deformations involving both normal and shear forces and exhibit unknown regional variation in stiffness, fiber alignment, and fiber orientation. Because the objective of the novel protocols presented here is at direct odds with the goals of most traditional biaxial tests aiming to characterize isotropic, homogeneous materials (Aydin et al., 2017; Lee, Fung, Shabetai, & LeWinter, 1987; Nemavhola, 2017; Rivlin, 1948; Rivlin & Saunders, 1951; Sacks, 2000), there are key differences from traditional methods. First, our biaxial testing protocol (Basic Protocol 1) was specifically designed to include multiple asymmetric mechanical tests in order to generate inhomogeneous strain fields and high levels of in-plane shear. Next, we rely on clamps, rather than the more standard use of sutures, to secure samples to load cells and to transfer motion from the actuators to the borders of the sample itself (Billiar & Sacks, 2000b; Debes & Fung, 1995; Humphrey, Strumpf, & Yin, 1990; Lee et al., 1987; Nemavhola, 2017, 2021). Unlike sutures, clamps do not allow the sample to rotate at the boundaries, facilitating the generation of shear boundary forces. Thirdly, we do not assume a constant sample thickness, but instead obtain full-field thickness measurements via laser micrometry (Basic Protocol 2). These three sets of data—full-field displacement, enhanced boundary force information, and full-field thickness—can be combined to yield detailed spatial descriptions of mechanics. Spatially varying material properties could then be fitted to a constitutive model via a number of successful inverse techniques (Davis, Luo, Avril, Duprey, & Lu, 2015; Katia Genovese, Casaletto, Humphrey, & Lu, 2014; Kroon & Holzapfel, 2008; Seshaiyer & Humphrey, 2003; Shih et al., 2021; Witzenburg, Raghupathy, Kren, Taylor, & Barocas, 2012; Zhao, Chen, & Lu, 2009, 2011).

Technological advancement drives our ability to obtain information about the non-negligible shear forces and strains arising during the biaxial testing of anisotropic, heterogeneous materials (Billiar & Sacks, 2000; Humphrey et al., 1990; Sacks, 2000). Developments in the field of digital image correlation (DIC) now allow for quick and affordable determinations of full-field displacements (Dong & Pan, 2017; Sutton, Wolters, Peters, Ranson, & McNeill, 1983), enabling measurement of the complex strain fields imposed. Six-degrees-of-freedom (6DOF) load cells capable of measuring both normal and shear forces throughout testing are now commercially available. Imaging methods, like laser micrometry, can capture full-field thickness contours of organic samples. Furthermore, the coupling of 2D mechanical characterizations with 3D thickness contours allows for a more accurate depiction of stress distributions in the tissue, supporting the identification of possible mechanical or structural heterogeneity. In short, our protocols, which utilize commercially available and accessible equipment, work to develop a detailed

26911299, 2022, 7, Downloaded from https://currentprotocols.onlinelibrary.wiley.com/doi/10.1002/cpz1.493 by University of Wisconsin,Madison Cam Department of Pathology and, Wiley Online Library on [19/12/2022]. See the Terms and Conditions (https://onlinelibrary.wiley.com/terms-and-conditions) on Wiley Online Library for rules of use; OA articles are governed by the applicable Creative Commons License

description of regional mechanics in soft tissue samples exhibiting nonlinear, anisotropic, and heterogeneous mechanical behavior through the use of novel clamping, loading, and boundary force acquisition strategies.

In Basic Protocol 1, we describe how to conduct a series of biaxial tests that produce full-field displacements and normal and shear boundary forces for soft tissues or soft tissue analogs that enable mechanical characterization of the sample. Basic Protocol 2, as well as Support Protocols 1 and 2, provides useful preparatory steps that maximize the utility and quality of biaxial testing results. In particular, Basic Protocol 2 details how to measure full-field sample thickness, Support Protocol 1 describes sample cutting and speckle pattern generation for DIC, and Support Protocol 2 provides steps for attaching the sample to the tester using a custom gripping system designed to minimize sample handling.

NOTE: When handling soft tissues or biologically derived soft tissue analogs, nitrile gloves should be worn.

UNIQUE BIAXIAL TESTING OF SOFT TISSUES AND TISSUE ANALOGS

BASIC PROTOCOL 1

Basic Protocol 1 describes how to biaxially test anisotropic, heterogeneous soft tissues and soft tissue analogs. The testing sequence is intended to induce multiple heterogeneous strain states. If conducted properly, this protocol will result in arm normal and shear forces as well as full-field displacement data. If desired, the data can be fitted using an inverse method to parameterize the sample's mechanical behavior according to a constitutive model or strain-energy function selected to accurately reflect the sample's behavior under the prescribed loading conditions. Parameterizations have been achieved using neo-Hookean, Mooney-Rivlin, Fung exponential, and Holzapfel-Gasser-Ogden strain-energy functions (Davis et al., 2015; Katia Genovese et al., 2014; Kroon & Holzapfel, 2008; Raghupathy & Barocas, 2010; Raghupathy, Witzenburg, Lake, Sander, & Barocas, 2011; Seshaiyer & Humphrey, 2003; Shih et al., 2021; Witzenburg et al., 2012; Zhao et al., 2009, 2011).

Materials

Speckled and clamped cruciform-shaped soft tissue sample (see Support Protocols 1 and 2)
0.01 M phosphate-buffered saline (PBS; ∼6 L)

Desktop computer (referenced biaxial system requires Intel i5-8500 processor and 16 GB RAM or better)
Biaxial testing system, containing:
  Actuators [e.g., TestResources, E216SP Electro Dynamic Actuator; four (4)]
  Load cells: one-degree-of-freedom (1DOF) load cells [e.g., TestResources, WF12S Miniature Fatigue Resistant Submersible IP65 Load Cells; two (2)] and 6DOF load cells [e.g., ATI, Nano 17 IP68 F/T Transducers; two (2)]
  1DOF software (e.g., TestResources, B8-16 TestBuilder and MTL32-2020)
  6DOF software (e.g., National Instruments LabVIEW 2019)
  Control software (e.g., TestResources, B8-16 TestBuilder)
Camera (e.g., Imperx, PoE-C2400, 2464 × 2056 pixels, 5 megapixels, 36 fps), with lens (e.g., Computar, M3Z1228C-MP) and image capture software (e.g., Imperx, IpxPlayer)
Isolation table (e.g., Thorlabs PFA51504 and B4860U)
Watertight acrylic bath
Connectors [3D printed or machined; four (4); STL Files 1 to 4 are provided in Supporting Information]
Gripping system (see Support Protocol 2)

26911299, 2022, 7, Downloaded from https://currentprotocols.onlinelibrary.wiley.com/doi/10.1002/cpz1.493 by University of Wisconsin,Madison Cam Department of Pathology and, Wiley Online Library on [19/12/2022]. See the Terms and Conditions (https://onlinelibrary.wiley.com/terms-and-conditions) on Wiley Online Library for rules of use; OA articles are governed by the applicable Creative Commons License

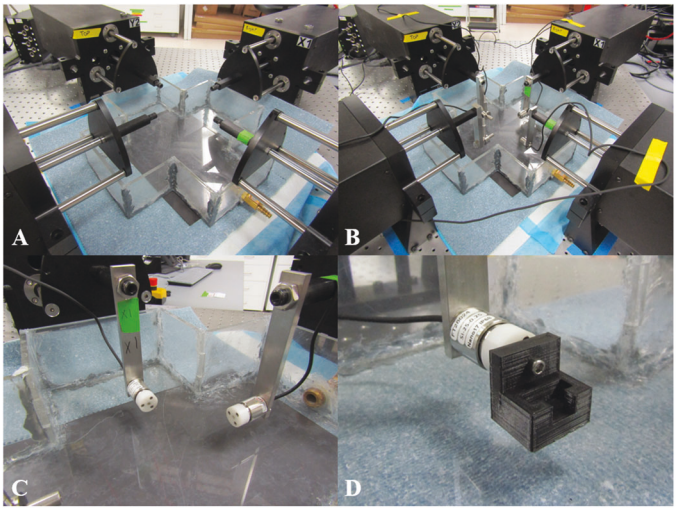

Figure 1 (**A**) Prior to testing, an empty bath should be placed in the center of the biaxial testing system. To aid in image clarity, a colored background may be placed under the bath, and to prevent accidental leaks, an underpad/spill pad may be placed between the bath and the isolation table. (**B**) Attach the load cells to the actuators and turn them on ≥30 min prior to testing. The amount of time necessary to warm up the load cells will vary between manufacturers. (**C**) Positioning of the 6DOF load cells on adjacent arms enables measurement of in-plane shear forces throughout the test. The inability to measure shear forces is a limitation of many planar biaxial testing systems. (**D**) Grip connector attached to a 6DOF load cell.

Prior to biaxial testing

1. At least 30 min before the desired testing time, turn on desktop computer, biaxial testing system, and camera. Confirm that isolation table, upon which the biaxial testing system is secured, is functional and ready for use.

   Different systems may require different warm-up periods. Consult the manufacturer.

2. Ensure that there is enough space on hard drive for data files generated during testing.

   At a resolution of ∼2400 pixels by ∼2000 pixels and a frame rate of 7 images per second, the testing protocol produces ∼50 GB of data. This size will vary based on the level of prescribed displacement and the displacement rate. We typically impose between 5% and 20% strain on each arm at a rate of ∼1%/s.

3. Place empty watertight acrylic bath in the center of the actuators (see Fig. 1A).

4. Attach load cells to their appropriate actuators (see Fig. 1B and 1C).

5. Zero the load cells.

   Monitor the cells for ∼10 min to ensure that readings do not drift substantially (more than ∼0.2 N) from zero. If the readings drift outside of the load cells' manufacturer's tolerance level, attempt to recalibrate them. If this does not resolve the issue, the load cells may be damaged and/or malfunctional and require service or replacement.

6. While carefully monitoring the applied forces in the 1DOF and 6DOF control softwares, attach a connector to each load cell (see Fig. 1D).

   Soft tissues typically require cells with low load ranges. Therefore, careful handling is necessary to prevent overloading and load cell damage.

7. Place speckled and clamped cruciform-shaped soft tissue sample in the gripping system and secure it to the biaxial testing system (see Support Protocol 2).

8. Slowly add 0.01 M PBS to bath.

26911299, 2022, 7, Downloaded from https://currentprotocols.onlinelibrary.wiley.com/doi/10.1002/cpz1.493 by University of Wisconsin,Madison Cam Department of Pathology and, Wiley Online Library on [19/12/2022]. See the Terms and Conditions (https://onlinelibrary.wiley.com/terms-and-conditions) on Wiley Online Library for rules of use; OA articles are governed by the applicable Creative Commons License

A layer of underpads and/or spill pads placed between the bath and the isolation table is useful for preventing leakage from reaching the table or actuators (see Fig. 1A).

9. Focus camera on the surface of the sample and adjust exposure so that the speckle pattern is sharp and well defined and has sufficient contrast between light and dark regions.

   A black or white background placed immediately beneath the bath may aid in identifying image sample boundaries. A discussion of speckling methods is included in the Commentary.

10. Add preload to tissue by incrementally moving the actuators outward in the control software.

    In general, preload should be ≤10% of the maximum load achieved during testing (Debes & Fung, 1995).

11. Set position of each actuator to zero.

    Once the position of the actuators has been set to zero, the resultant configuration of the sample will serve as the reference configuration for the following biaxial tests.

Conducting biaxial testing

12. Begin imaging sample surface and recording forces.

    Adjust the camera settings so that the sample is in focus and will not be out of frame when maximally extended. To record images of the sample, navigate to the data acquisition tab in the imaging software, set the desired imaging frequency (i.e., 7 Hz), ensure that the files are being written to the appropriate folder with a consistent naming convention, and, once satisfied, begin recording images. To record forces, locate the data acquisition window in the software for the 1DOF and 6DOF load cells. Create a new file for the test with a consistent naming convention, ensure that the forces are being sampled and recorded at a desirable rate (i.e., 100 Hz), and then begin recording and conduct the planned test.

13. Apply 10 equibiaxial stretch tests to sample at a rate of 1%/s for preconditioning such that the sample achieves a state of pseudoelasticity (Table 1).

    Preconditioning is commonly applied to tissue analogs and soft tissues such that they reach a state of pseudoelasticity characterized by repeatable force-displacement curves in response to the same loading conditions. The total amount of applied arm stretch, the rate of stretch, and the number of cycles necessary to achieve pseudoelasticity vary with sample type. In general, 10 equibiaxial stretches at the desired maximum strain level and a strain rate of 1%/s are sufficient to precondition tissue analogs and many soft tissues (Demer & Yin, 1983; Fung, Fronek, & Patitucci, 1979; Sacks, 2000).

14. To maximize both shear and normal strains, conduct 15 different biaxial tests in which stretch is applied to different sample arms (Table 1).

    Note that for stiffer or softer samples, load cells with different ranges and tolerances than those specified may be required.

15. Conduct one final equibiaxial stretch test (Table 1).

    Results from this test can be compared with earlier equibiaxial extensions to confirm that the sample maintained pseudoelasticity and sustained minimal damage during testing.

16. Repeat steps 13 through 15 for additional imposed arm displacement levels if desired.

    For new sample types, it is useful to conduct testing at increasing amounts and/or rates of arm displacement to avoid tearing the sample prematurely. An applied strain of 5%-10% is often a safe starting point. We utilize a strain rate of 1%/s (Sacks, 2000).

26911299, 2022, 7, Downloaded from https://currentprotocols.onlinelibrary.wiley.com/doi/10.1002/cpz1.493 by University of Wisconsin,Madison Cam Department of Pathology and, Wiley Online Library on [19/12/2022]. See the Terms and Conditions (https://onlinelibrary.wiley.com/terms-and-conditions) on Wiley Online Library for rules of use; OA articles are governed by the applicable Creative Commons License

Table 1 Mechanical Tests Utilized in Basic Protocol 1

Test	Setup	Displacement ratio[a]
Preconditioning	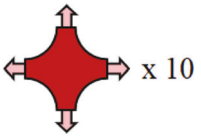 x 10	1:1:1:1
Equibiaxial	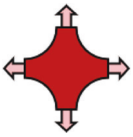	1:1:1:1
Two-arm pull	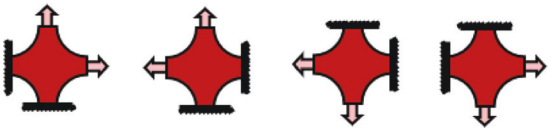	1:1:0:0 0:1:1:0 0:0:1:1 1:0:0:1
Single-arm pull	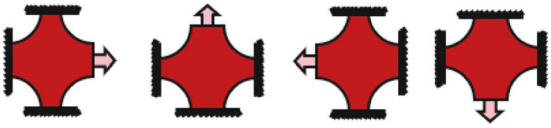	1:0:0:0 0:1:0:0 0:0:1:0 0:0:0:1
Strip biaxial	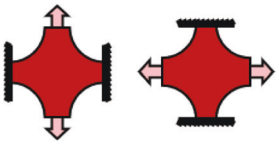	0:1:0:1 1:0:1:0
Three-arm pull	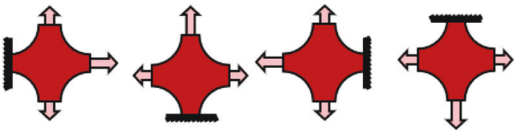	1:0.67:0:0.67 0.67:1:0.67:0 0:0.67:1:0.67 0.67:0:0.67:1
Equibiaxial	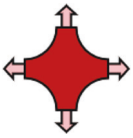	1:1:1:1

[a] Displacement ratios are given as right arm:top arm:left arm:bottom arm. A displacement ratio of 1 indicates the maximum prescribed displacement, 0 indicates no displacement, and values between 0 and 1 are a percentage of the maximum displacement (e.g., 0.67 is 67% of the maximum displacement).

Following biaxial testing

17. Drain PBS from the bath.
18. Remove sample and gripping system from the tester while carefully monitoring the forces applied to the load cells in the 1DOF and 6DOF softwares.
19. Remove connectors from each load cell.
20. Remove and clean load cells.

    If load cells are repeatedly exposed to PBS, it is important to rinse all surfaces in distilled water to avoid corrosion. Follow the manufacturer's instructions for load cell disassembly and cleaning.

21. Dispose of sample appropriately.

26911299, 2022, 7, Downloaded from https://currentprotocols.onlinelibrary.wiley.com/doi/10.1002/cpz1.493 by University of Wisconsin-Madison Cam Department of Pathology and, Wiley Online Library on [19/12/2022]. See the Terms and Conditions (https://onlinelibrary.wiley.com/terms-and-conditions) on Wiley Online Library for rules of use; OA articles are governed by the applicable Creative Commons License

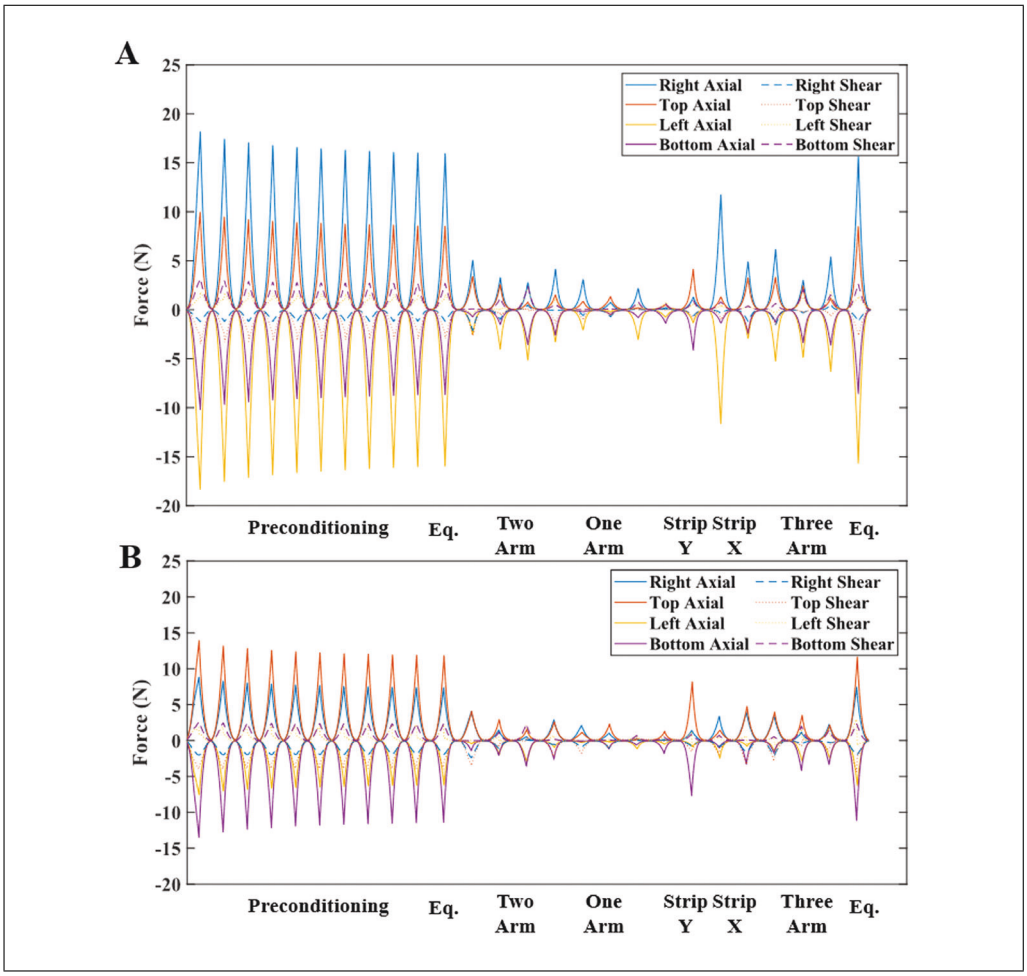

Figure 2 (**A**) Boundary forces throughout the biaxial testing protocol detailed in Basic Protocol 1 for a TissueMend sample oriented with its stiffest axis aligned along the *x*-axis of the biaxial testing system. Measured normal forces are depicted by solid lines, measured shear forces are plotted with dashed lines, and the remaining calculated shear forces (computed assuming static equilibrium) are represented by dotted lines. Table 1 details different biaxial tests. (**B**) Boundary forces throughout the same biaxial testing protocol for a different TissueMend sample oriented so that its stiffest axis was offset by 45° from the *x*-axis of the testing system. Shear forces, again indicated by dashed and dotted lines, were more prominent for this sample. The measurement of shear forces at the sample boundary is a central goal of Basic Protocol 1.

IMPORTANT NOTE: *Follow local rules and regulations. Soft tissues may be considered hazardous waste. We deposit animal-derived soft tissue samples containing no pathogens into a plastic container and store it in a –20°C freezer. Once filled, we insert the container into a plastic bag, place the bag in a cardboard box, and seal the box. Boxes are retrieved and disposed of by the University of Wisconsin-Madison Department of Environment, Health, and Safety.*

22. Sanitize laboratory surfaces and system components.

IMPORTANT NOTE: *Again, follow local rules and regulations for soft tissue handling. Isopropyl alcohol and bleach are commonly used disinfectants. Sharps should be placed in an appropriate container and disposed of according to institutional protocols.*

Data analysis

23. Perform data analysis as desired.

Completion of Basic Protocol 1 produces boundary forces for the prescribed extensions and raw images of the deforming sample's surface throughout the extensions. We create a 2D mesh of the sample's surface with quadrilateral elements using Abaqus.

26911299, 2022, 7, Downloaded from https://currentprotocols.onlinelibrary.wiley.com/doi/10.1002/cpz1.493 by University of Wisconsin,Madison Cam Department of Pathology and, Wiley Online Library on [19/12/2022]. See the Terms and Conditions (https://onlinelibrary.wiley.com/terms-and-conditions) on Wiley Online Library for rules of use; OA articles are governed by the applicable Creative Commons License

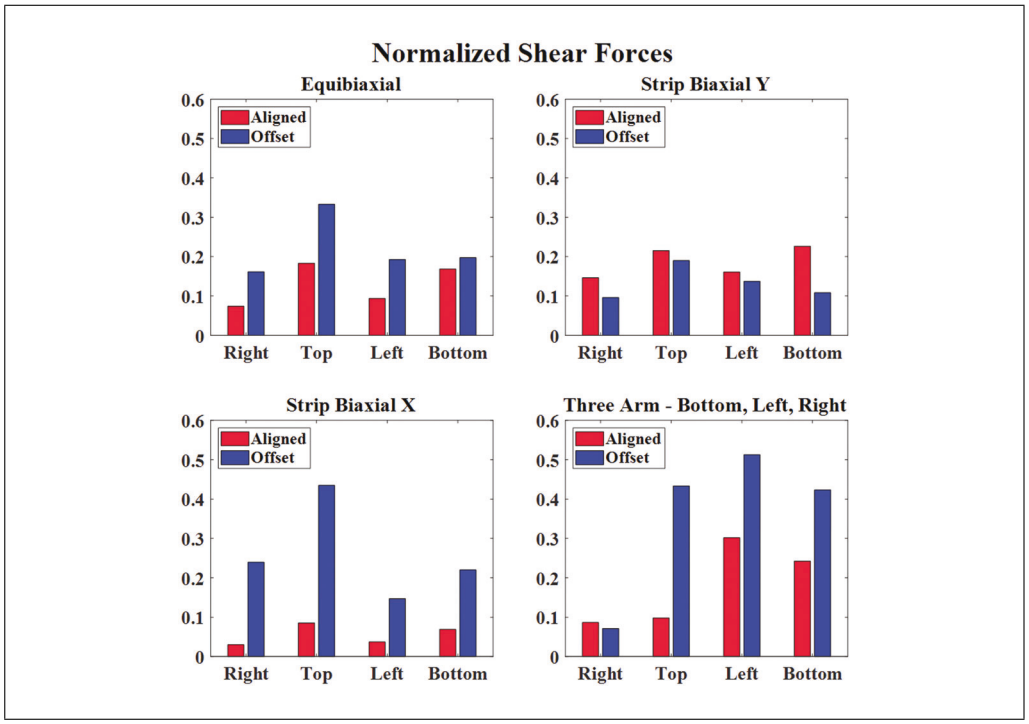

Figure 3 Shear forces along the right, top, left, and bottom arms of each TissueMend cruciform sample normalized with respect to the largest force measured during each extension (only the equibiaxial, *y*-axis strip biaxial, *x*-axis strip biaxial, and bottom-left-right extensions are shown). In the symmetric extensions, shear forces were small for the aligned sample (<23%) and sometimes larger for the offset sample (up to 44%). For the asymmetric extension, shear strains were larger for both samples; however, they were much larger for the offset sample.

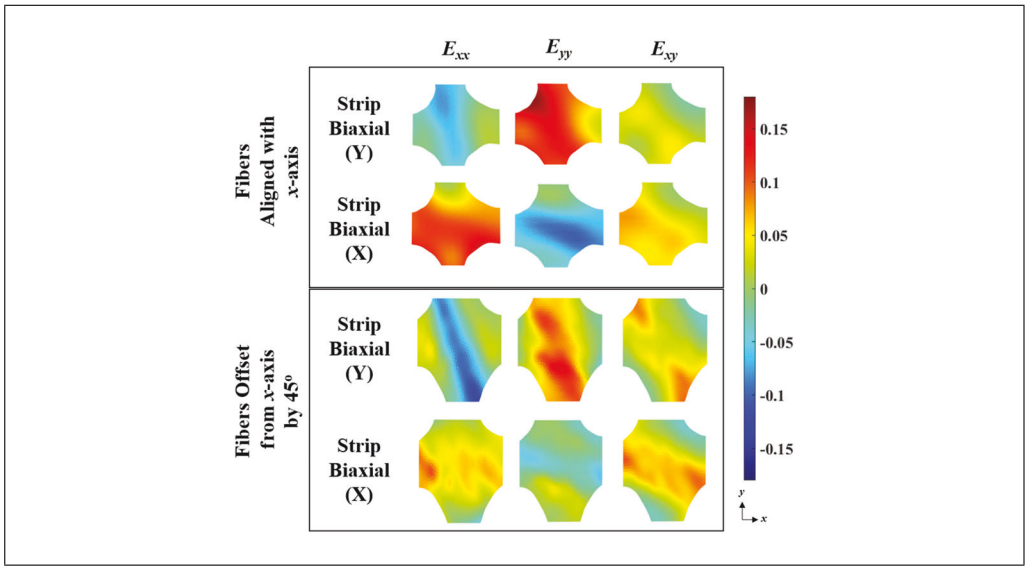

Figure 4 Green strain contours produced by processing sample images from Basic Protocol 1 using DIC for the strip biaxial extensions (Raghupathy & Barocas, 2013). For a TissueMend sample that had its stiffest direction aligned with the *x*-axis of our testing system (top), relatively homogeneous strain distributions can be seen, as can the shear strain contours that, for the most part, are nearly an order of magnitude smaller than their normal counterparts. For the TissueMend sample that was aligned so that its stiffest direction was offset from the *x*-axis by 45° (bottom), shear strain was increased overall, and there was increased spatial heterogeneity for all three strain measures. The measurement of heterogeneous normal and shear strain fields is a central goal of Basic Protocol 1 and can be used to identify regions of varying stiffness and anisotropy in samples. The DIC code utilized for this analysis is available at *https://license.umn.edu/product/robust-image-correlation-based-strain-calculator-for-tissue-systems*.

26911299, 2022, 7, Downloaded from https://currentprotocols.onlinelibrary.wiley.com/doi/10.1002/cpz1.493 by University of Wisconsin,Madison Cam Department of Pathology and, Wiley Online Library on [19/12/2022]. See the Terms and Conditions (https://onlinelibrary.wiley.com/terms-and-conditions) on Wiley Online Library for rules of use; OA articles are governed by the applicable Creative Commons License

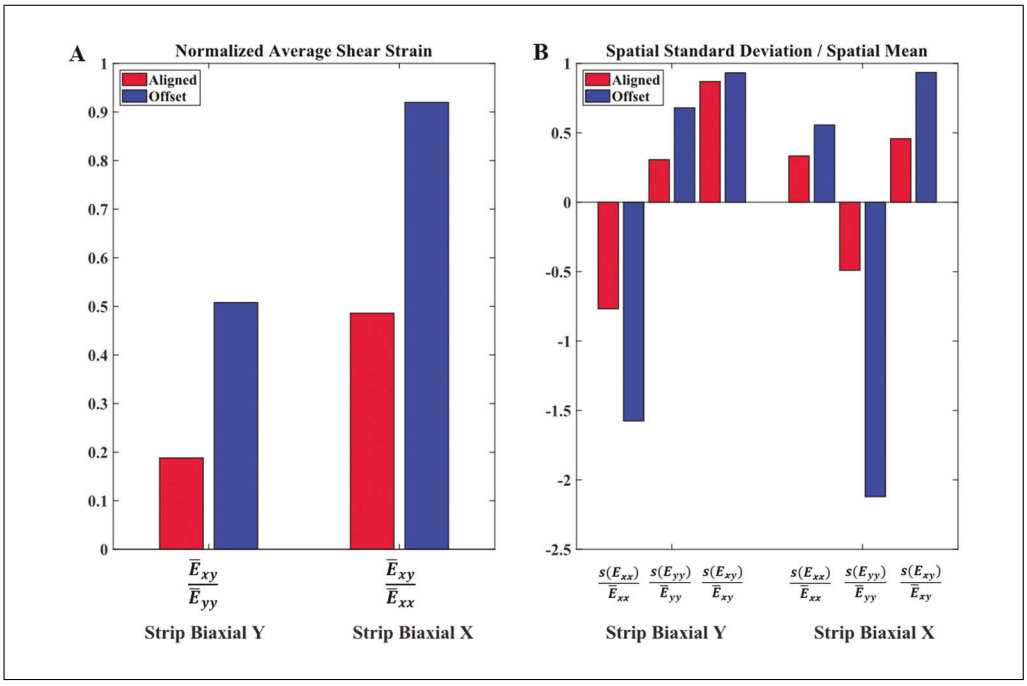

Figure 5 (**A**) To compare strain magnitudes, the average spatial shear strain was calculated throughout the two TissueMend samples and divided by the average maximum spatial normal strain for the strip biaxial tests in the *x* and *y* directions. For both extensions, the offset TissueMend sample exhibited larger normalized shear strains. (**B**) To quantify heterogeneity, the spatial standard deviation of each strain component was divided by its respective spatial mean (Witzenburg et al., 2012). The offset TissueMend sample exhibited increased heterogeneity for all three Green strain components for both strip biaxial extensions.

Then, we apply DIC to compute full-field displacement and strain (Raghupathy & Barocas, 2013). This DIC code is available at https://license.umn.edu/product/robust-image-correlation-based-strain-calculator-for-tissue-systems. Boundary forces and full-field displacements can then be used to construct load-displacement or stress-strain plots or input into a more advanced inverse mechanical analysis to identify material parameters.

Figure 2 shows arm forces throughout our biaxial testing protocol (Table 1) for TissueMend samples aligned along the horizontal axis of the biaxial testing machine and aligned at ∼45° from the test axis. TissueMend (TEI Biosciences and Stryker Corporation) is a surgical patch composed of non-denatured, non-crosslinked collagen derived from fetal bovine skin. This analog is a Class II FDA-approved material for soft tissue (e.g., rotator cuff, patellar, and Achilles tendon) repair surgeries. We normalized the shear forces to the maximum force for each extension to compare the samples quantitatively in Figure 3. Figure 4 depicts Green strain contours for these two samples at maximum extension for the strip biaxial tests. We computed the spatial averages and standard deviations of strain to compare the strain contours measured in the TissueMend samples quantitatively in Figure 5. Together, these figures demonstrate the primary advantages of our protocol to produce and measure shear forces at a sample's boundary, pronounced heterogeneity in the strain fields, and large shear strains. Additionally, Video 1 in the Supporting Information shows the equibiaxial extension of the TissueMend sample aligned along the horizontal axis of the biaxial tester.

FULL-FIELD THICKNESS MEASUREMENT OF SOFT TISSUES AND TISSUE ANALOGS

BASIC PROTOCOL 2

Basic Protocol 2 describes a technique for measuring the full-field thickness of a soft tissue or soft tissue analog. It is especially useful for samples with varying thicknesses or pronounced heterogeneity. The biaxial testing protocol discussed earlier (see Basic Protocol 1) produces 2D forces and full-field displacement data. In combination with

26911299, 2022, 7, Downloaded from https://currentprotocols.onlinelibrary.wiley.com/doi/10.1002/cpz1.493 by University of Wisconsin-Madison Cam Department of Pathology and, Wiley Online Library on [19/12/2022]. See the Terms and Conditions (https://onlinelibrary.wiley.com/terms-and-conditions) on Wiley Online Library for rules of use; OA articles are governed by the applicable Creative Commons License

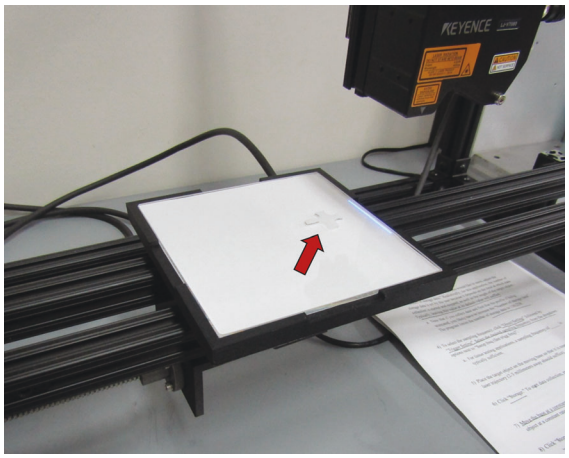

Figure 6 A translating stage moves the sample under the laser micrometer, generating a series of thickness profiles (Basic Protocol 2). A glass insert on top of a white piece of paper offers a consistent and easy-to-clean platform for the sample (indicated by the red arrow) to rest on during scanning.

these data, the full-field thicknesses obtained from this protocol enable quantification of sample stress.

Materials

Cruciform-shaped soft tissue sample (see Support Protocol 1)

Desktop computer (referenced biaxial system requires Intel i5-8500, 16 GB RAM or better)
Laser micrometer (e.g., Keyence, LJ-V7080), with software for laser micrometer visualization (e.g., LJ-Navigator 2 and LJ-Observer)
Motorized stage (e.g., motor: Applied Motion, NEMA 23 STM23Q-2AN; ball screw and nut: McMaster-Carr, 6641K1 and 6641K21), with motor control software (e.g., Applied Motion, ST Configurator; Applied Motion, Q Programmer)

Full-thickness measurement

1. Turn on desktop computer, laser micrometer, and motorized stage 30 min prior to use.

   Different systems may require different warm-up periods. Consult the manufacturer.

2. Zero out laser head by scanning the empty translating stage. Adjust for tilt of the laser or stage, if necessary.

3. Set desired laser scanning frequency (e.g., 20 Hz).

4. Place cruciform-shaped soft tissue sample onto the scanning stage in the desired orientation (see Fig. 6).

   Samples are scanned 2 min after removal from solution. Careful attention to and measurement of the time out of solution are necessary for soft tissues because evaporation can influence thickness measurement.

5. Use motorized stage to slowly translate the sample beneath the laser micrometer's head and then scan sample.

   Setting the profilometer to a frequency of 20 Hz and the motor speed to 1.55 mm/s yields 13 profiles per millimeter. The series of profiles are combined to produce full-field thickness measurements of the sample.

26911299, 2022, 7, Downloaded from https://currentprotocols.onlinelibrary.wiley.com/doi/10.1002/cpz1.493 by University of Wisconsin,Madison Cam Department of Pathology and, Wiley Online Library on [19/12/2022]. See the Terms and Conditions (https://onlinelibrary.wiley.com/terms-and-conditions) on Wiley Online Library for rules of use; OA articles are governed by the applicable Creative Commons License

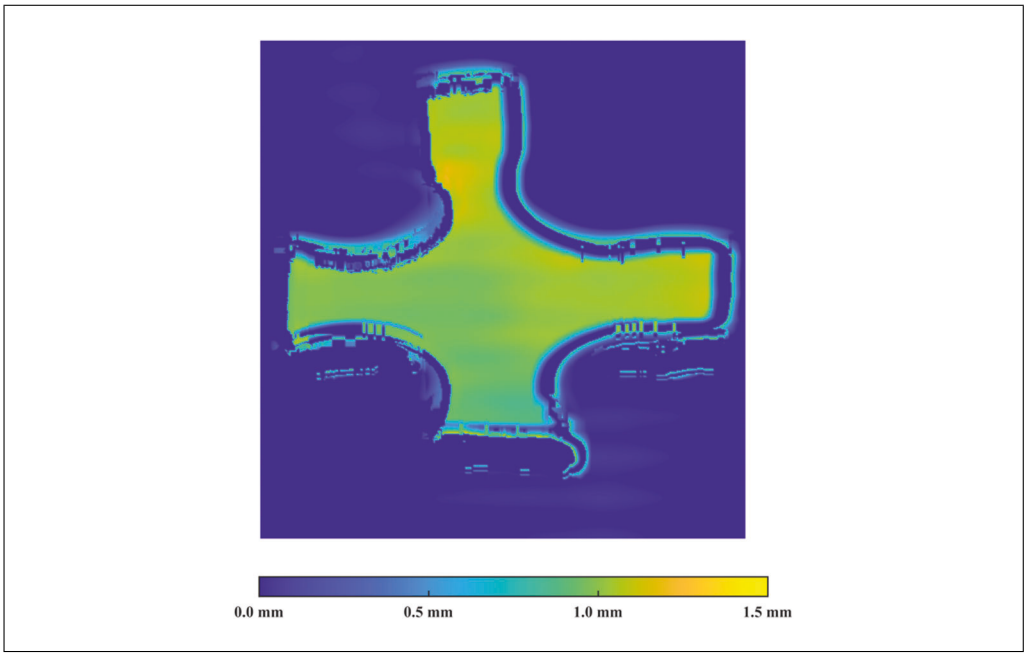

Figure 7 Example of the thickness contours obtained from Basic Protocol 2. In the central region of the hydrated TissueMend sample, the thickness was relatively uniform, at 0.995 ± 0.01 mm, suggesting homogeneity.

6. Remove tissue from the stage. Mechanically test, store, or dispose of sample appropriately.

   See the annotation to step 21 in Basic Protocol 1 for disposal information.

7. Power down laser and sanitize scanning stage.

   IMPORTANT NOTE: *Follow local rules and regulations for soft tissue. Isopropyl alcohol and bleach are common disinfectants.*

Data analysis

8. Perform data analysis as desired.

   Basic Protocol 2 produces an output file detailing the 3D sample geometry. Supporting Information, File 5, is a representative file corresponding to the horizontally aligned TissueMend sample imaged in Figure 7. Figure 7 shows a visualization of the full-field thickness and volume of a TissueMend sample determined via laser micrometry. To produce the image in Figure 7, the output file was read into MATLAB, the stage level was set to zero, noise was removed using a Gaussian filter, and the 3D geometry was visualized as a surface. Supporting Information, File 6, is the MATLAB code used to analyze the output file and produce surface plots of the sample's thickness.

CREATING AND SPECKLING CRUCIFORM-SHAPED SAMPLES FOR MECHANICAL TESTING

SUPPORT PROTOCOL 1

Support Protocol 1 details how to prepare soft tissue and soft tissue analog samples for biaxial testing (Basic Protocol 1). By definition, planar biaxial testing relies on the application of in-plane forces only, such that a state of plane stress can be assumed. For this assumption to be valid, samples must be thin. Because soft tissues are often naturally thin slabs, sheets, or membranes (Humphrey, 2002), planar biaxial testing is a common testing modality for soft tissues and tissue analogs. In general, it is recommended that samples undergoing biaxial testing have a thickness at least one order of magnitude less than their overall length and width (Ventsel & Krauthammer, 2001). Additionally, the *ex vivo* and planar nature of biaxial testing generally limits its application to quantification of passive tissue properties. Cruciform-shaped samples are commonly utilized in biaxial tests and lend themselves well to clamping (Support Protocol 2). To quantify full-field

26911299, 2022, 7, Downloaded from https://currentprotocols.onlinelibrary.wiley.com/doi/10.1002/cpz1.493 by University of Wisconsin,Madison Cam Department of Pathology and, Wiley Online Library on [19/12/2022]. See the Terms and Conditions (https://onlinelibrary.wiley.com/terms-and-conditions) on Wiley Online Library for rules of use; OA articles are governed by the applicable Creative Commons License

Figure 8 (**A**) Place the TissueMend in a petri dish, cover with room-temperature PBS, and allow 10 min for the sample to become fully hydrated. (**B**) Using a biopsy punch, remove the corners of the rectangular analog to create a roughly cruciform-shaped sample. (**C**) Use a razor blade to trim away excess material, yielding the desired cruciform shape.

deformations using DIC, texture is applied to the sample. Here, an approach utilizing an airbrush and India ink is detailed. It produces a fine, random texture that adheres to the sample surface without altering mechanics. After achieving a satisfactory sample shape and sufficient speckle pattern, the sample is ready for gripping and biaxial testing (Basic Protocol 1).

Materials

Soft tissue or soft tissue analog sample
0.01 M PBS (e.g., Sigma-Aldrich, P3813-10PAK; pH 7.4, ~50 ml)

Forceps (e.g., Fine Science Tools, 11053-10)
Cutting board
Biopsy punches (e.g., Robbins Instruments, Disposable, 10 mm Diameter, RBP-100)
Razor blades
100 × 15–mm petri dishes (e.g., VWR, 25384-302)
Airbrush (e.g., Master Airbrush G233) filled with India ink (e.g., Speedball Super Black India Ink 3378)
Air supply (~45 psi)

1. Remove soft tissue or soft tissue analog sample from storage and place in 0.01 M PBS.

   We recommend immersing TissueMend samples in room-temperature PBS for ~10 min for full hydration (see Fig. 8A).

2. Use forceps to move sample from PBS to the cutting board.

   Take note of the sample's orientation before and after cutting. This is critical for samples with prominent levels of anisotropy and/or heterogeneity.

3. Use a biopsy punch and razor blade to trim sample into a cruciform shape.

   Biopsy punches create smooth, curved edges near the sample center (see Fig. 8B). Razor blades can then be used to trim any small remnants and form sample arms (see Fig. 8C). Care should be exercised such that the final sample is sufficiently thin. Note the final sample in Figure 8C is ~20 mm in length and width, which is approximately 20 times the average thickness in Figure 7.

4. Return cruciform-shaped sample to PBS to prevent dehydration prior to testing.

5. Dispose of any trimmed remnants appropriately.

   IMPORTANT NOTE: *Follow local rules and regulations. Soft tissues may be considered hazardous waste. We deposit TissueMend remnants into a plastic container and store it in a –20°C freezer. Once filled, we insert the container into a plastic bag, place the bag in a cardboard box, and seal the box. Boxes are retrieved and disposed of by the University of Wisconsin-Madison Department of Environment, Health, and Safety.*

26911299, 2022, 7, Downloaded from https://currentprotocols.onlinelibrary.wiley.com/doi/10.1002/cpz1.493 by University of Wisconsin,Madison Cam Department of Pathology and, Wiley Online Library on [19/12/2022]. See the Terms and Conditions (https://onlinelibrary.wiley.com/terms-and-conditions) on Wiley Online Library for rules of use; OA articles are governed by the applicable Creative Commons License

6. Place sample in an empty 100 × 15–mm petri dish and speckle sample using an airbrush filled with India ink with an appropriate air supply.

   The airbrush technique can be difficult to implement initially and requires practice. Hold the airbrush ∼6 in. away from the sample and spray lightly. Continue spraying the sample in bursts until the desired speckle pattern has been achieved. After speckling, allow ≥10 min for the dye to dry. This is important for maintaining the integrity of the speckle pattern once the sample is placed in PBS for mechanical testing. We use a spray nozzle that is 0.2 to 0.3 mm in diameter and attach the airbrush to an air supply at 30 to 50 psi.

   Support Protocol 1 produces a cruciform-shaped sample with a high-quality speckle pattern that can be biaxially tested using Basic Protocol 1. Proper handling and careful trimming are necessary to create a sample with clean, smooth edges that reduce the likelihood of tearing during testing. The speckle patterns applied to samples should follow the general guidelines for speckling intended for strain tracking via DIC, which are outlined in more detail in the Background Information section of the Commentary.

7. Sanitize instruments and laboratory surfaces.

   IMPORTANT NOTE: *Follow local rules and regulations for soft tissue. Isopropyl alcohol and bleach are common disinfectants. Sharps (i.e., razor blades and biopsy punches) should be placed in an appropriate container and disposed of according to institutional protocol.*

CUSTOM GRIPPING SYSTEM TO MINIMIZE SAMPLE HANDLING

SUPPORT PROTOCOL 2

This protocol describes how a custom gripping system is used to attach a small soft tissue or soft tissue analog sample to a biaxial testing machine (Basic Protocol 1). The specialized gripping system was designed such that a sample could be secured using a stereoscope, away from the testing machine. This gripping system utilizes clamps to secure the sample, rather than sutures, rakes, or hooks, to induce in-plane shear during biaxial testing.

Materials

All-purpose Krazy Glue (∼2 g)
Cruciform-shaped soft tissue sample (see Support Protocol 1)

Water-resistant sandpaper (e.g., McMaster-Carr, 4660A14)
Custom gripping system (3D printed or machined; STL Files 1 to 4 are provided in Supporting Information), containing:
  Bottom clamps (4)
  Base (1)
  Large thumb screws (e.g., McMaster-Carr, 99607A142)
  Top clamps (4)
  Small socket head screws (e.g., McMaster-Carr, 92196A108)
  Connectors (4)
  Small thumb screws (e.g., McMaster-Carr, 91185A257)
Hex-key Allen wrench set

1. Prior to testing, cut small rectangular pieces of water-resistant sandpaper and glue them to bottom clamps between the threaded holes in the custom gripping system using all-purpose Krazy Glue.

   Sandpaper helps eliminate slipping or pinching of the sample. Small dabs of Krazy Glue are sufficient for bonding the sandpaper to the grips. The glue should dry within 10 min but takes ∼24 hr to fully cure.

2. Attach bottom clamps to the base with large thumb screws using a hex-key Allen wrench set (see Fig. 9A).

26911299, 2022, 7, Downloaded from https://currentprotocols.onlinelibrary.wiley.com/doi/10.1002/cpz1.493 by University of Wisconsin,Madison Cam Department of Pathology and, Wiley Online Library on [19/12/2022]. See the Terms and Conditions (https://onlinelibrary.wiley.com/terms-and-conditions) on Wiley Online Library for rules of use; OA articles are governed by the applicable Creative Commons License

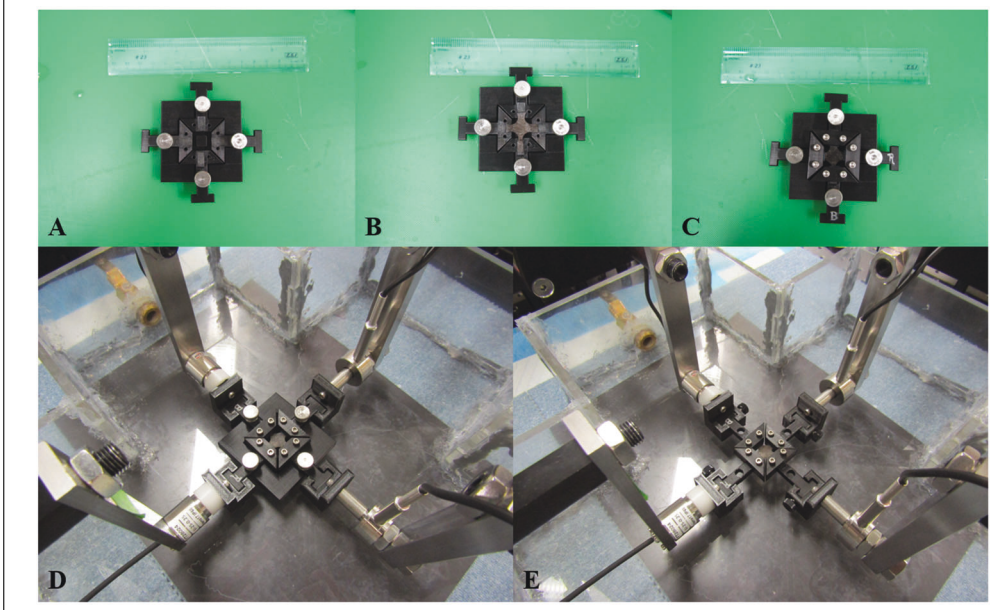

Figure 9 (**A**) The bottom clamps are attached to the base with large thumb screws. Strips of sandpaper can be seen on each of the bottom clamps. (**B**) Each of the speckled TissueMend sample's four arms are placed such that the sample rests on the strips of sandpaper glued to the bottom clamps. (**C**) Top clamps are attached to the bottom clamps using the small socket head screws. Although not visible, sandpaper strips are also glued to the surface of the top clamps that come into contact with the sample. (**D**) The clamped and secured sample is placed into the connectors attached to the biaxial testing machine. At this point, the base is still in place. (**E**) The gripping system without the supportive base. Each bottom clamp is secured to a connector using a small thumb screw, and then the base is removed.

3. Place cruciform-shaped soft tissue sample on the bottom clamps and base. Take note of sample orientation.

   See Figure 9B. Support Protocol 1 details the sample preparation.

4. Secure top clamps on the sample using small socket head screws (see Fig. 9C).

5. Place "T"-shaped ends of the bottom clamps into the connectors (see Fig. 9D).

   Carefully monitor the applied forces to avoid damaging the load cells. The connectors were attached to the biaxial testing system load cells in step 6 of Basic Protocol 1.

6. Secure each bottom clamp to a connector using a small thumb screw and then slowly remove base (see Fig. 9E).

   Once the clamps are attached to the connectors and the base has been removed, the sample is secured in the biaxial testing machine (see Basic Protocol 1, step 7). The gripping system now enables motion from the actuator to transfer to each sample arm during biaxial testing.

   Support Protocol 2 outlines our procedure for off-machine clamping of soft tissue or tissue analog samples intended for biaxial testing. The custom gripping system (Files 1 to 4 in the Supporting Information) was designed to limit sample handling and reduce damage risk. It is simple to produce and implement and enables samples to be quickly and safely connected to the biaxial testing machine (see Basic Protocol 1, step 7).

COMMENTARY

Background Information

Biaxial testing of soft, highly deformable samples was popularized in the 1940s and 1950s, coinciding with the development of polymers. Treloar described methods for generating simple, homogeneous strain fields in thin sheets of rubber (Treloar, 1948), and Rivlin & Saunders (Rivlin, 1948; Rivlin &

26911299, 2022, 7, Downloaded from https://currentprotocols.onlinelibrary.wiley.com/doi/10.1002/cpz1.493 by University of Wisconsin,Madison Cam Department of Pathology and, Wiley Online Library on [19/12/2022]. See the Terms and Conditions (https://onlinelibrary.wiley.com/terms-and-conditions) on Wiley Online Library for rules of use; OA articles are governed by the applicable Creative Commons License

Saunders, 1951) proposed and demonstrated energy theories for large, homogeneous deformations of incompressible materials like rubber. The overarching themes of this early biaxial testing—specifically, homogeneous deformations of highly elastic and incompressible materials—were quickly adapted for soft biological tissues. Early biaxial tests (Lanir & Fung, 1974a, 1974b) revealed hallmark characteristics of soft tissues that differentiate them from other materials, including nonlinear force-displacement relationships, pronounced hysteresis, and mechanical anisotropy. Throughout the next two decades, biaxial testing was conducted on many different soft tissues, including skin (Alexander & Cook, 1977; Meijer, Douven, & Oomens, 1999; Schneider, Davidson, & Nahum, 1984), bladders (Gloeckner, Sacks, Chancellor, & deGroat, 1999; Gloeckner et al., 2002; Nagatomi, Chancellor, & Sacks, 2003), arteries (Chuong & Fung, 1986; Chuong & Fung, 1983; Dobrin & Canfield, 1984; Fung et al., 1979), heart valves (Billiar & Sacks, 2000; Lo & Vesely, 1995; Stella & Sacks, 2007), pericardium (Chew, Yin, & Zeger, 1986; Lee, Lewinter, Freeman, Shabetai, & Fung, 1985; Lee et al., 1987), endocardium and epicardium (Humphrey et al., 1990; Kang, Humphrey, & Yin, 1996), and myocardium (Demer & Yin, 1983; Sacks & Chuong, 1993; Yin, Strumpf, Chew, & Zeger, 1987). From these studies, foundational principles integral to the biaxial testing of soft tissues arose, including preconditioning and pseudoelasticity (Fung et al., 1979; Tong & Fung, 1976), residual stresses (Chuong & Fung, 1986), and exponential strain energy functions and strain-stiffening behavior (Choi & Vito, 1990; Guccione, McCulloch, & Waldman, 1991; Tong & Fung, 1976). In addition to these more general concepts, tissue-specific practices also developed. For example, skin typically exhibits pseudoelasticity following three preconditioning cycles (Zeng et al., 2004), whereas cardiovascular samples often require 8 to 10 cycles of preconditioning (Demer & Yin, 1983; Fung et al., 1979; Weizsäcker, Lambert, & Pascale, 1983). In contrast, tendons exhibit more prominent viscoelastic behavior and are typically preconditioned using cyclic stress-relaxation tests (McGough, Debski, Taskiran, Fu, & Woo, 2013; Sverdlik & Lanir, 2002).

During biaxial testing, in-plane shear forces can arise naturally from the inherent anisotropy and heterogeneous composition of a tissue's intricate and dynamic extracellular matrix (Humphrey, Dufresne, & Schwartz, 2014). To manage this issue, biomechanists developed strategies to limit the presence of these forces, some of which include aligning a specimen's primary fiber direction along testing axes and using sutures, rather than clamps, to connect the sample to the testing machine (Jacobs, Cortes, Vresilovic, & Elliott, 2013; Jiang, Sridhar, Robbins, Freed, & Moreno, 2021; Sacks, 2000; Sun, Sacks, & Scott, 2005). Sutures allow rotation at the sample boundaries, ensuring force application perpendicular to the sample's boundary. Unfortunately, they also introduce damage to the sample and create stress concentrations around the puncture sites (Cilla, Corral, Peña, & Peña, 2020; Eilaghi, Flanagan, Brodland, & Ethier, 2009; Sun et al., 2005). A few biomechanists have created custom systems with larger numbers of actuators and load cells to actually measure in-plane shear forces (Khalsa, Hoffman, & Grigg, 1996; Malcolm, Nielsen, Hunter, & Charette, 2002). However, the increased cost and complexity of these systems have limited their broader use (Sacks, 2000). The combination of commercially available 6DOF load cells and biaxial testing machines reduces these concerns while enabling measurement of in-plane shear forces.

Much like in-plane shear forces, inhomogeneous displacement fields occur commonly in soft tissues due to existing heterogeneity and anisotropy. Because the fundamental theories presented by Rivlin, Saunders, Treloar, and other rubber experts relied on homogeneous deformation and strain fields (Jones & Treloar, 1975; Rivlin & Saunders, 1951; Treloar, 1948), a common approach for soft tissues is to consider only a small central region of the soft tissue specimen when computing deformation and strain and to assume homogeneity within that region (Deplano et al., 2016; Eilaghi et al., 2009). Strategic placement of markers on the sample surface facilitates this approach (Hoffman & Grigg, 1984; Humphrey, Vawter, & Vito, 1987; Thomopoulos, Fomovsky, & Holmes, 2005). Full-field displacement measurements can be made to evaluate and validate the location, size, and presence of a supposed homogeneous strain region (Haddadi & Belhabib, 2008; Palanca, Tozzi, & Cristofolini, 2016). The most commonly applied technique used to assess full-field strains and displacements of a material is DIC (Quino et al., 2020). DIC utilizes cross-correlation algorithms to

26911299, 2022, 7, Downloaded from https://currentprotocols.onlinelibrary.wiley.com/doi/10.1002/cpz1.493 by University of Wisconsin,Madison Cam Department of Pathology and, Wiley Online Library on [19/12/2022]. See the Terms and Conditions (https://onlinelibrary.wiley.com/terms-and-conditions) on Wiley Online Library for rules of use; OA articles are governed by the applicable Creative Commons License

determine matching subsets of two consecutive images obtained during mechanical testing (Chu, Peters, Ranson, & Sutton, 1982; Chu, Ranson, & Sutton, 1985; Dong & Pan, 2017; Sutton et al., 1983). This approach has undergone immense advancements driven by the development of digital cameras, affordable and accessible computing power, and efficient, automated cross-correlation algorithms. Along with these innovations, the contactless, non-destructive nature of DIC makes it particularly attractive for soft biological tissues.

The accuracy and resolution of DIC depend largely on the quality of the speckle pattern produced on a sample's surface. In general, high-quality speckle patterns are random and isotropic (Yang, Tao, & Franck, 2021), exhibit stark contrast from the sample's base coloring (Reu, 2015), are finely distributed [Reu (2014) suggests speckles that are approximately 3 to 5 pixels in size], and adhere well to the sample's surface without altering its mechanical behavior (Quino et al., 2020). Generating a robust speckle pattern on hydrated, highly deformable soft tissues is challenging, and there is no consensus on the best method. Aerosolization is one common technique used for speckling soft biological tissues (Berfield et al., 2007; Crammond, Boyd, & Dulieu-Barton, 2011; Lionello & Cristofolini, 2014; Lionello, Sirieix, & Baleani, 2014; Zhou et al., 2016). For airbrush systems, the size and distribution of speckles depend on nozzle diameter, distance between the sample and the nozzle, air pressure, and viscosity of the dye (Dong & Pan, 2017). Given the lighter color of soft tissues, dark dyes, such as India ink, Verhoeff's stain, methylene blue, or Cancer Diagnostics tissue staining dye, are common (Katia Genovese, Montes, Martínez, & Evans, 2015; Lake & Barocas, 2012; Luyckx et al., 2014; Myers, Coudrillier, Boyce, & Nguyen, 2010; Walsh et al., 2020; Witzenburg et al., 2012; Zhou et al., 2016). Conversely, if the tissue is darker in color, a lighter-colored dye may be appropriate (Barranger, Doumalin, Dupré, & Germaneau, 2010; Palanca et al., 2016). Temporary tattoo ink and water-slide paper are less common dye application methods that enable reproducible patterns (Quino et al., 2020). Dyes are suitable for large deformations because they adhere to the sample surface, but it can be challenging to produce fine patterns, and the stiffness and volume of the dye should be minimized to avoid altering mechanics (Crammond et al., 2011). Powders such as graphite powder are also commonly used to speckle biological samples (Myers et al., 2010; Wang, Xie, Li, & Zhu, 2012). When applied, they create fine patterns with little impact on mechanics but often adhere poorly to tissue surfaces. Thus, powders can be challenging to utilize when deformations are large or when samples are immersed in fluid (Palanca et al., 2016). Other novel techniques for creating high-quality speckle patterns utilize lithography (Tanaka, Yang, Liu, & Kagawa, 2007), focused ion beams (Zhu, Xie, Xue, Wang, & Li, 2015), and surface abrasion (Dong, Kakisawa, & Kagawa, 2015). For more information on recent developments in DIC and speckle pattern fabrication, reviews by Dong & Pan and Palanca et al. are recommended (Dong & Pan, 2017; Palanca et al., 2016).

Following the successful completion of the protocols described here, spatial material properties could be fitted to the full-field displacement data, boundary forces, and full-field thicknesses produced utilizing an inverse approach. A variety of inverse techniques have been implemented in direct, iterative, and pointwise manners to model soft tissue mechanics (Davis et al., 2015; Katia Genovese et al., 2014; Kroon & Holzapfel, 2008; Seshaiyer & Humphrey, 2003; Zhao et al., 2009, 2011). In the past, we have developed and applied a generalized anisotropic inverse mechanics method to estimate regional differences in stiffness and mechanical anisotropy (Raghupathy & Barocas, 2010; Raghupathy et al., 2011; Shih et al., 2021; Witzenburg et al., 2012), but the resultant data from this novel technique are of independent value, and their analysis need not be limited to our inverse method.

Load-bearing tissues rely on the incredible complexity of their microstructure for proper function. Thus, there has been a broad effort to characterize their mechanical behavior. Importantly, adaptation to local changes in loading involves regional remodeling, such that even healthy tissues often display spatial variation in mechanical behavior and properties. A barrier to investigating the heterogeneous nature of soft tissues is the lack of experimental protocols and analysis tools that can accurately capture these spatial variations in whole-tissue specimens. Fortunately, new testing techniques and technology are enabling more detailed, full-field measurements of tissue behavior, such as digital volume correlation (Luetkemeyer, Cai, Neu, & Arruda, 2018; Midgett et al., 2016) and omnidirectional DIC

26911299, 2022, 7, Downloaded from https://currentprotocols.onlinelibrary.wiley.com/doi/10.1002/cpz1.493 by University of Wisconsin,Madison Cam Department of Pathology and, Wiley Online Library on [19/12/2022]. See the Terms and Conditions (https://onlinelibrary.wiley.com/terms-and-conditions) on Wiley Online Library for rules of use; OA articles are governed by the applicable Creative Commons License

(Genovese, 2019). Here, we present a unique biaxial testing protocol (Basic Protocol 1) designed to generate in-plane shear forces and inhomogeneous strain fields. Our protocol leverages commercially available mechanical testing equipment—namely, electrodynamic actuators, axial and 6DOF load cells, and high-resolution imaging systems—to capture 3D, undeformed sample geometry as well as full-field deformation and axial and shear forces during a series of unique biaxial extensions.

Critical Parameters

A critical aspect of this set of protocols is sample handling, which depends largely on the type of tissue or tissue analog. TissueMend, for example, is a more robust analog than collagen gels, which require more delicate handling. Rough or notched sample edges often lead to tearing during biaxial extension (Basic Protocol 1). We suggest using biopsy punches to generate smooth curved sample edges in one motion. Custom gripping systems (Support Protocol 2), like the one presented here, can also reduce handling-related damage.

A high-quality speckle pattern is necessary for accurate quantification of displacements and strains throughout the biaxial testing protocol (Basic Protocol 1). Applying speckle patterns to soft tissues (Support Protocol 1) can be challenging, especially if the tissue must be hydrated throughout preparation and testing. Removing a speckle pattern from a soft tissue or tissue analog is often not possible, and small adjustments to air pressure, the distance from the sample, and the amount of dye or powder released can greatly affect the final speckle pattern. It is wise to fine-tune these parameters on affordable materials prior to speckling valuable or limited specimens. Estrada & Franck have developed a fast, user-friendly, open-source MATLAB code to analyze the quality of speckle patterns for several different deformation types that may be useful for quantitatively assessing pattern quality (Estrada & Franck, 2015).

We suggest careful consideration of overall tissue stiffness and physiologic loading when selecting the range and resolution of both 1DOF and 6DOF load cells. If the maximum capacity of the cell is exceeded, it may break, requiring costly replacement. However, as the maximum force capacity increases, the signal-to-noise ratio is reduced. Load cells should also be properly maintained to ensure accurate measurement of normal and in-plane shear forces. Regular calibration according to manufacturer standards is recommended. PBS is highly corrosive, and even immersible stainless steel load cells will rust if not properly cleaned between testing sessions.

Troubleshooting

Table 2 includes potential problems that may arise during the implementation of the protocols presented. This collection of problems is not comprehensive but does include issues that we have faced and overcome with moderate success.

Understanding Results

The planar biaxial testing protocol described in Basic Protocol 1 generates images of the sample surface throughout testing and normal and shear arm forces for a thin cruciform-shaped tissue or tissue analog. Figure 2 shows the measured normal and shear boundary forces for two different representative TissueMend samples: one aligned such that its stiffest axis was along the x-axis of the testing system and one such that its stiffest axis was offset by 45° from the x-axis of the testing system. To compare these samples, we plotted the shear forces along the right, top, left, and bottom arms normalized to the largest force measured during each extension (Fig. 3). For the symmetric extensions (equibiaxial and strip biaxial extensions), the aligned sample exhibited small shear forces that were $<23\%$ of the maximum normal force. Shear forces were generally larger for the offset sample for these extensions, approaching 44% of the maximum normal force in some cases. Notably, shear forces were very large for the offset sample during asymmetric extensions ($>50\%$ of the maximum normal force) and approached 30% of the maximum normal force even for the aligned sample. These results demonstrate that the use of 6DOF load cells results in robust measurement of both normal and shear forces, potentially enabling biaxial testing of samples with unknown or heterogeneous fiber alignments or anisotropy.

Using DIC software, full-field displacements and strains were computed from the images of the sample surface obtained during Basic Protocol 1. Figure 4 shows Green strain contours for the strip biaxial extensions for the two representative TissueMend samples tested and discussed in Figures 2 and 3. We computed the spatial averages and standard deviations of strain to compare the strain contours measured in the TissueMend samples quantitatively. Shear strain increased about 2-fold for the offset sample, and heterogeneity was increased in

26911299, 2022, 7, Downloaded from https://currentprotocols.onlinelibrary.wiley.com/doi/10.1002/cpz1.493 by University of Wisconsin,Madison Cam Department of Pathology and, Wiley Online Library on [19/12/2022]. See the Terms and Conditions (https://onlinelibrary.wiley.com/terms-and-conditions) on Wiley Online Library for rules of use; OA articles are governed by the applicable Creative Commons License

Table 2 Troubleshooting Guide for the Planar Biaxial Testing of Soft Tissues and Soft Tissue Analogs

Problem	Possible cause	Solution
Damaged sample	Improper handling	Exercise more caution next time; explore alternative tissue analogs (if applicable)
Sample slipping during biaxial testing	Clamps not secured	Ensure clamps are fully tightened down prior to testing
Floating speckle during biaxial testing	Speckle pattern was not allowed to dry long enough; poor speckling material	Allow ≥10 min for speckle pattern to dry; use pipets to remove as much excess speckle as possible; experiment with other materials and techniques
Unrealistic thickness measurements	Laser micrometer not zeroed out properly	Calibrate laser micrometer prior to measurements; adjust in post-processing
Unrealistic displacement fields	Low-quality speckle pattern; floating speckle	Allow ≥10 min for speckle pattern to dry; use pipets to remove as much excess speckle as possible; computationally deform sample and confirm strain with DIC code
Unrealistic force signals	Improperly calibrated load cells; broken load cells	If possible, calibrate load cells in-house; otherwise, send load cells to manufacturer for evaluation, calibration, and repair

every strain component (Fig. 5). There are a number of DIC codes available for use (e.g., Blaber, Adair, & Antoniou, 2015; Solav, Moerman, Jaeger, Genovese, & Herr, 2018; Yang & Bhattacharya, 2019a, 2019b). For the strain contours shown in Figure 4, we used a code developed especially for soft tissues (Raghupathy & Barocas, 2013). It is available at *https://license.umn.edu/product/robust-image-correlation-based-strain-calculator-for-tissue-systems*. Prior to testing soft biological tissues, the direction of fiber alignment, stiffness, and composition of the sample are rarely known. Our biaxial testing protocol generates heterogeneous strain fields as well as elevated shear strains so that samples can be mechanically characterized regardless of their orientation or constituents.

A series of thickness profiles was stored and saved by the laser during scanning, as described in Basic Protocol 2. Utilizing the motor speed, the set of profiles was converted from a function of time to a function of distance, smoothed using a Gaussian filter, and merged together to create full-field thickness contours of the scanned sample via a custom MATLAB code (Supporting Information, File 6). Figure 7 shows the full-field thickness of the TissueMend sample aligned such that its stiffest axis was along the *x*-axis of the testing system. Given that TissueMend is a commercially available product intended to replicate the behavior and appearance of tendons, it is likely that the homogeneous thickness is favorable.

Time Considerations

In total, these protocols require approximately 4 to 5 hr. Biaxial testing (Basic Protocol 1) requires ∼2 hr to complete, but timing will vary based on the number of testing rounds, the prescribed strain, and the strain rate. For example, one round of testing to 10% prescribed strain at 1%/s can be conducted faster than multiple rounds of testing at higher strains and lower strain rates. Rapid completion (about 2 to 3 min) of thickness measurements (Basic Protocol 2) is recommended to avoid dehydration effects. Preparing, speckling, gripping, and securing the sample into the testing machine (Support Protocols 1 and 2) can be slow, taking up to 2 hr, but are critical to the success of biaxial testing. For frozen tissue, additional time will be needed for thawing.

Acknowledgments

This work was funded by a grant from the National Science Foundation Division of Civil, Mechanical and Manufacturing Innovation (ID, 2030173) to C.M.W. The authors would also like to thank Michael Chiariello, Elizabeth Gunderson, Jiujiu Pan, Riley Pieper, and Shreya Sreedhar for their assistance on various projects that have made these protocols possible.

Author Contributions

Daniel Pearce: Conceptualization, Data curation, Formal analysis, Investigation, Methodology, Visualization, Writing—original draft, Writing—review

26911299, 2022, 7, Downloaded from https://currentprotocols.onlinelibrary.wiley.com/doi/10.1002/cpz1.493 by University of Wisconsin,Madison Cam Department of Pathology and, Wiley Online Library on [19/12/2022]. See the Terms and Conditions (https://onlinelibrary.wiley.com/terms-and-conditions) on Wiley Online Library for rules of use; OA articles are governed by the applicable Creative Commons License

and editing; **Mark Nemcek**: Methodology, Writing—original draft, Writing—review and editing; **Colleen Witzenburg**: Conceptualization, Data curation, Formal analysis, Funding acquisition, Investigation, Methodology, Project administration, Resources, Software, Supervision, Visualization, Writing—original draft, Writing—review and editing.

Conflict of Interest

The authors declare no conflict of interest.

Data Availability Statement

The data, 3D part files, and materials (product numbers and vendors) that support the protocol are available in the Supporting Information or from the corresponding author upon request.

Literature Cited

Alexander, H., & Cook, T. H. (1977). Accounting for natural tension in the mechanical testing of human skin. *Journal of Investigative Dermatology*, *69*(3), 310–314. doi: 10.1111/1523-1747.ep12507731

Aydin, R. C., Brandstaeter, S., Braeu, F. A., Steigenberger, M., Marcus, R. P., Nikolaou, K., … Cyron, C. J. (2017). Experimental characterization of the biaxial mechanical properties of porcine gastric tissue. *Journal of the Mechanical Behavior of Biomedical Materials*, *74*, 499–506. doi: 10.1016/j.jmbbm.2017.07.028

Barranger, Y., Doumalin, P., Dupré, J. C., & Germaneau, A. (2010). Digital image correlation accuracy: Influence of kind of speckle and recording setup. *EPJ Web of Conferences*, *6*, 31002. doi: 10.1051/EPJCONF/20100631002

Berfield, T. A., Patel, J. K., Shimmin, R. G., Braun, P. V., Lambros, J., & Sottos, N. R. (2007). Micro-and nanoscale deformation measurement of surface and internal planes via digital image correlation. *Experimental Mechanics*, *47*(1), 51–62. doi: 10.1007/S11340-006-0531-2

Billiar, K. L., & Sacks, M. S. (2000). Biaxial mechanical properties of the natural and glutaraldehyde treated aortic valve cusp—Part I: Experimental results. *Journal of Biomechanical Engineering*, *122*(1), 23–30. doi: 10.1115/1.429624

Blaber, J., Adair, B., & Antoniou, A. (2015). Ncorr: Open-source 2D digital image correlation Matlab software. *Experimental Mechanics*, *55*(6), 1105–1122. doi: 10.1007/S11340-015-0009-1/FIGURES/14

Chew, P. H., Yin, F. C. P., & Zeger, S. L. (1986). Biaxial stress-strain properties of canine pericardium. *Journal of Molecular and Cellular Cardiology*, *18*(6), 567–578. doi: 10.1016/S0022-2828(86)80965-8

Choi, H. S., & Vito, R. P. (1990). Two-dimensional stress-strain relationship for canine pericardium. *Journal of Biomechanical Engineering*, *112*(2), 153–159. doi: 10.1115/1.2891166

Chu, T., Peters, W. H., Ranson, W. F., & Sutton, M. A. (1982). Application of digital correlation methods to rigid body mechanics. *Proceedings of the Society for Experimental Stress Analysis*, 73–76. doi: 10.1117/12.7973231

Chu, T. C., Ranson, W. F., & Sutton, M. A. (1985). Applications of digital-image-correlation techniques to experimental mechanics. *Experimental Mechanics*, *25*(3), 232–244. doi: 10.1007/BF02325092

Chuong, C., & Fung, Y. (1986). On residual stresses in arteries. *Journal of Biomechanical Engineering*, *108*(2), 189–192. doi: 10.1115/1.3138600

Chuong, C. J., & Fung, Y. C. (1983). Three–dimensional stress distribution in arteries. *Journal of Biomechanical Engineering*, *105*(3), 268–274. doi: 10.1115/1.3138417

Cilla, M., Corral, A. V., Peña, J. A., & Peña, E. (2020). Analysis of the accuracy on computing nominal stress in a biaxial test for arteries. *Strain*, *56*(1), e12331. doi: 10.1111/STR.12331

Claeson, A. A., & Barocas, V. H. (2017). Planar biaxial extension of the lumbar facet capsular ligament reveals significant in-plane shear forces. *Journal of the Mechanical Behavior of Biomedical Materials*, *65*, 127–136. doi: 10.1016/J.JMBBM.2016.08.019

Crammond, G., Boyd, S. W., & Dulieu-Barton, J. M. (2011). Speckle pattern characterisation for high resolution digital image correlation. *Applied Mechanics and Materials*, *70*, 261–266. doi: 10.4028/WWW.SCIENTIFIC.NET/AMM.70.261

Davis, F., Luo, Y., Avril, S., Duprey, A., & Lu, J. (2015). Pointwise characterization of the elastic properties of planar soft tissues: Application to ascending thoracic aneurysms. *Biomechanics and Modeling in Mechanobiology*, *14*, 967–978. doi: 10.1007/s10237-014-0646-9

Debes, J., & Fung, Y. (1995). Biaxial mechanics of excised canine pulmonary arteries. *The American Journal of Physiology*, *269*, H433–42. doi: 10.1152/AJPHEART.1995.269.2.H433

Demer, L. L., & Yin, F. C. (1983). Passive biaxial mechanical properties of isolated canine myocardium. *The Journal of Physiology*, *339*(1), 615–630. doi: 10.1113/jphysiol.1983.sp014738

Deplano, V., Boufi, M., Boiron, O., Guivier-Curien, C., Alimi, Y., & Bertrand, E. (2016). Biaxial tensile tests of the porcine ascending aorta. *Journal of Biomechanics*, *49*(10), 2031–2037. doi: 10.1016/J.JBIOMECH.2016.05.005

Dobrin, P. B., & Canfield, T. R. (1984). Elastase, collagenase, and the biaxial elastic properties of dog carotid artery. *The American Journal of Physiology*, *247*, H124–31. doi: 10.1152/Ajpheart.1984.247.1.H124

Dong, Y., Kakisawa, H., & Kagawa, Y. (2015). Development of microscale pattern for digital image correlation up to 1400°C. *Optics and Lasers in Engineering*, *68*, 7–15. doi: 10.1016/J.OPTLASENG.2014.12.003

Dong, Y. L., & Pan, B. (2017). A review of speckle pattern fabrication and assessment for

26911299, 2022, 7, Downloaded from https://currentprotocols.onlinelibrary.wiley.com/doi/10.1002/cpz1.493 by University of Wisconsin,Madison Cam Department of Pathology and, Wiley Online Library on [19/12/2022]. See the Terms and Conditions (https://onlinelibrary.wiley.com/terms-and-conditions) on Wiley Online Library for rules of use; OA articles are governed by the applicable Creative Commons License

digital image correlation. *Experimental Mechanics*, *57*(8), 1161–1181. doi: 10.1007/s11340-017-0283-1

Eilaghi, A., Flanagan, J. G., Brodland, G. W., & Ethier, C. R. (2009). Strain uniformity in biaxial specimens is highly sensitive to attachment details. *Journal of Biomechanical Engineering*, *131*(9), 091003. doi: 10.1115/1.3148467/459881

Estrada, J. B., & Franck, C. (2015). Intuitive interface for the quantitative evaluation of speckle patterns for use in digital image and volume correlation techniques. *Journal of Applied Mechanics*, *82*(9), 095001. doi: 10.1115/1.4030821

Fung, Y., Fronek, K., & Patitucci, P. (1979). Pseudoelasticity of arteries and the choice of its mathematical expression. *Heart and Circulatory Physiology*, *6*(5), H620–31. doi: 10.1152/AJPHEART.1979.237.5.H620

Gardiner, J. C., & Weiss, J. A. (2001). Simple shear testing of parallel-fibered planar soft tissues. *Journal of Biomechanical Engineering*, *123*(2), 170–175. doi: 10.1115/1.1351891

Genovese, K. (2019). An omnidirectional DIC system for dynamic strain measurement on soft biological tissues and organs. *Optics and Lasers in Engineering*, *116*, 6–18. doi: 10.1016/J.OPTLASENG.2018.12.006

Genovese, K., Casaletto, L., Humphrey, J. D., & Lu, J. (2014). Digital image correlation-based pointwise inverse characterization of heterogeneous material properties of gallbladder in vitro. *Proceedings of the Royal Society A: Mathematical, Physical and Engineering Sciences*, *470*(2167), 20140152. doi: 10.1098/rspa.2014.0152

Genovese, K., Montes, A., Martínez, A., & Evans, S. L. (2015). Full-surface deformation measurement of anisotropic tissues under indentation. *Medical Engineering and Physics*, *37*(5), 484–493. doi: 10.1016/j.medengphy.2015.03.005

Gloeckner, D., Sacks, M., Chancellor, M., & De Groat, W. (1999). Active and passive biaxial mechanical properties of urinary bladder wall. *Annual International Conference of the IEEE Engineering in Medicine and Biology - Proceedings*, *1*, 17. doi: 10.1109/IEMBS.1999.802036

Gloeckner, D. C., Sacks, M. S., Fraser, M. O., Somogyi, G. T., De Groat, W. C., & Chancellor, M. B. (2002). Passive biaxial mechanical properties of the rat bladder wall after spinal cord injury. *Journal of Urology*, *167*(5), 2247–2252. doi: 10.1016/S0022-5347(05)65137-3

Guccione, J. M., McCulloch, A. D., & Waldman, L. K. (1991). Passive material properties of intact ventricular myocardium determined from a cylindrical model. *Journal of Biomechanical Engineering*, *113*(1), 42–55. doi: 10.1115/1.2894084

Haddadi, H., & Belhabib, S. (2008). Use of rigid-body motion for the investigation and estimation of the measurement errors related to digital image correlation technique. *Optics and Lasers in Engineering*, *46*(2), 185–196. doi: 10.1016/J.OPTLASENG.2007.05.008

Hoffman, A. H., & Grigg, P. (1984). A method for measuring strains in soft tissue. *Journal of Biomechanics*, *17*(10), 795–800. doi: 10.1016/0021-9290(84)90110-6

Humphrey, J. D., Strumpf, R. K., & Yin, F. C. P. (1990). Biaxial mechanical behavior of excised ventricular epicardium. *American Journal of Physiology - Heart and Circulatory Physiology*, *259*, H101–8. doi: 10.1152/AJPHEART.1990.259.1.H101

Humphrey, J. D., Vawter, D. L., & Vito, R. P. (1987). Quantification of strains in biaxially tested soft tissues. *Journal of Biomechanics*, *20*(1), 59–65. doi: 10.1016/0021-9290(87)90267-3

Humphrey, J. D. (2002). *Cardiovascular solid mechanics*. New York: Springer. doi: 10.1007/978-0-387-21576-1

Humphrey, J. D., Dufresne, E. R., & Schwartz, M. A. (2014). Mechanotransduction and extracellular matrix homeostasis. *Nature Reviews Molecular Cell Biology*, *15*(12), 802–812. doi: 10.1038/nrm3896

Jacobs, N. T., Cortes, D. H., Vresilovic, E. J., & Elliott, D. M. (2013). Biaxial tension of fibrous tissue: Using finite element methods to address experimental challenges arising from boundary conditions and anisotropy. *Journal of Biomechanical Engineering*, *135*(2), 1–10. doi: 10.1115/1.4023503

Jiang, M., Sridhar, R. L., Robbins, A. B., Freed, A. D., & Moreno, M. R. (2021). A versatile biaxial testing platform for soft tissues. *Journal of the Mechanical Behavior of Biomedical Materials*, *114*, 104144. doi: 10.1016/J.JMBBM.2020.104144

Jones, D. F., & Treloar, L. R. G. (1975). The properties of rubber in pure homogeneous strain. *Journal of Physics D: Applied Physics*, *8*(11), 1285. doi: 10.1088/0022-3727/8/11/007

Kang, T., Humphrey, J. D., & Yin, F. C. P. (1996). Comparison of biaxial mechanical properties of excised endocardium and epicardium. *American Journal of Physiology - Heart*, *270*, H2169–76. doi: 10.1152/ajpheart.1996.270.6.H2169

Khalsa, P. S., Hoffman, A. H., & Grigg, P. (1996). Mechanical states encoded by stretch-sensitive neurons in feline joint capsule. *Journal of Neurophysiology*, *76*(1), 175–187. doi: 10.1152/Jn.1996.76.1.175

Kroon, M., & Holzapfel, G. A. (2008). Estimation of the distributions of anisotropic, elastic properties and wall stresses of saccular cerebral aneurysms by inverse analysis. *Proceedings of the Royal Society A: Mathematical, Physical and Engineering Sciences*, *464*(2092), 807–825. doi: 10.1098/rspa.2007.0332

Lake, S. P., & Barocas, V. H. (2012). Mechanics and kinematics of soft tissue under indentation are determined by the degree of initial collagen fiber alignment. *Journal of the Mechanical Behavior of Biomedical Materials*, *13*, 25–35. doi: 10.1016/j.jmbbm.2012.03.017

26911299, 2022, 7, Downloaded from https://currentprotocols.onlinelibrary.wiley.com/doi/10.1002/cpz1.493 by University of Wisconsin,Madison Cam Department of Pathology and, Wiley Online Library on [19/12/2022]. See the Terms and Conditions (https://onlinelibrary.wiley.com/terms-and-conditions) on Wiley Online Library for rules of use; OA articles are governed by the applicable Creative Commons License

Lanir, Y., & Fung, Y. C. (1974a). Two-dimensional mechanical properties of rabbit skin—I. Experimental system. *Journal of Biomechanics*, *7*(1), 29–34. doi: 10.1016/0021-9290(74)90067-0

Lanir, Y., & Fung, Y. C. (1974b). Two-dimensional mechanical properties of rabbit skin—II. Experimental results. *Journal of Biomechanics*, *7*(2), 171–182. doi: 10.1016/0021-9290(74)90058-X

Lee, M., Lewinter, M. M., Freeman, G., Shabetai, R., & Fung, Y. C. (1985). Biaxial mechanical properties of the pericardium in normal and volume overload dogs. *Heart and Circulatory Physiology*, *18*(2), H222–H230. doi: 10.1152/ajpheart.1985.249.2.H222

Lee, M. C., Fung, Y. C., Shabetai, R., & Le Winter, M. M. (1987). Biaxial mechanical properties of human pericardium and canine comparisons. *The American Journal of Physiology*, *253*, H75–82. doi: 10.1152/Ajpheart.1987.253.1.H75

Lionello, G., & Cristofolini, L. (2014). A practical approach to optimizing the preparation of speckle patterns for digital-image correlation. *Measurement Science and Technology*, *25*(10), 107001. doi: 10.1088/0957-0233/25/10/107001

Lionello, G., Sirieix, C., & Baleani, M. (2014). An effective procedure to create a speckle pattern on biological soft tissue for digital image correlation measurements. *Journal of the Mechanical Behavior of Biomedical Materials*, *39*, 1–8. doi: 10.1016/J.JMBBM.2014.07.007

Lo, D., & Vesely, I. (1995). Biaxial strain analysis of the porcine aortic valve. *The Annals of Thoracic Surgery*, *60*(SUPPL. 2), S374–S378. doi: 10.1016/0003-4975(95)00249-K

Luetkemeyer, C. M., Cai, L., Neu, C. P., & Arruda, E. M. (2018). Full-volume displacement mapping of anterior cruciate ligament bundles with dualMRI. *Extreme Mechanics Letters*, *19*, 7–14. doi: 10.1016/J.EML.2017.12.004

Luyckx, T., Verstraete, M., De Roo, K., De Waele, W., Bellemans, J., & Victor, J. (2014). Digital image correlation as a tool for three-dimensional strain analysis in human tendon tissue. *Journal of Experimental Orthopaedics*, *1*(1), 1–9. doi: 10.1186/s40634-014-0007-8

Malcolm, D. T. K., Nielsen, P. M. F., Hunter, P. J., & Charette, P. G. (2002). Strain measurement in biaxially loaded inhomogeneous, anisotropic elastic membranes. *Biomechanics and Modeling in Mechanobiology*, *1*(3), 197–210. doi: 10.1007/S10237-002-0018-8

McGough, R. L., Debski, R. E., Taskiran, E., Fu, F. H., & Woo, S. L. Y. (2013). Mechanical properties of the long head of the biceps tendon. *Knee Surgery, Sports Traumatology, Arthroscopy*, *3*(4), 226–229. doi: 10.1007/BF01466622

Meijer, R., Douven, L. F. A., & Oomens, C. W. J. (1999). Characterisation of anisotropic and nonlinear behaviour of human skin in vivo. *Computer Methods in Biomechanics and Biomedical Engineering*, *2*(1), 13–27. doi: 10.1080/10255849908907975

Midgett, D. E., Quigley, H. A., Pease, M. E., Franck, C., Toyjanova, J., Nguyen, T. D., … Toyjanova, J. (2016). Inflation test of the human optic nerve head using digital volume correlation. *Conference Proceedings of the Society for Experimental Mechanics Series*, *6*, 7–15. doi: 10.1007/978-3-319-21455-9_2

Myers, K. M., Coudrillier, B., Boyce, B. L., & Nguyen, T. D. (2010). The inflation response of the posterior bovine sclera. *Acta Biomaterialia*, *6*(11), 4327–4335. doi: 10.1016/J.ACTBIO.2010.06.007

Nagatomi, J., Chancellor, M. B., & Sacks, M. S. (2003). Active biaxial mechanical properties of bladder wall tissue. *American Society of Mechanical Engineers, Bioengineering Division (Publication) BED*, *55*, 341–342. doi: 10.1115/IMECE2003-43146

Nemavhola, F. (2017). Biaxial quantification of passive porcine myocardium elastic properties by region. *Engineering Solid Mechanics*, *5*, 155–166. doi: 10.5267/j.esm.2017.6.003

Nemavhola, F. (2021). Study of biaxial mechanical properties of the passive pig heart: Material characterisation and categorisation of regional differences. *International Journal of Mechanical and Materials Engineering*, *16*, 1–14. doi: 10.1186/s40712-021-00128-4

Palanca, M., Tozzi, G., & Cristofolini, L. (2016). The use of digital image correlation in the biomechanical area: A review. *International Biomechanics*, *3*(1), 1–21. doi: 10.1080/23335432.2015.1117395

Quino, G., Chen, Y., Ramakrishnan, K. R., Martínez-Hergueta, F., Zumpano, G., Pellegrino, A., & Petrinic, N. (2020). Speckle patterns for DIC in challenging scenarios: Rapid application and impact endurance. *Measurement Science and Technology*, *32*(1), 015203. doi: 10.1088/1361-6501/ABAAE8

Raghupathy, R., & Barocas, V. H. (2010). Generalized anisotropic inverse mechanics for soft tissues. *Journal of Biomechanical Engineering*, *132*(8), 081006. doi: 10.1115/1.4001257

Raghupathy, R., & Barocas, V. H. (2013). *Robust Image Correlation Based Strain Calculator for Tissue Systems (20130022, Dr. Victor Barocas)*. Retrieved from https://license.umn.edu/product/robust-image-correlation-based-strain-calculator-for-tissue-systems

Raghupathy, R., Witzenburg, C., Lake, S. P., Sander, E. A., & Barocas, V. H. (2011). Identification of regional mechanical anisotropy in soft tissue analogs. *Journal of Biomechanical Engineering*, *133*(9), 091011. doi: 10.1115/1.4005170

Reu, P. (2014). All about speckles: Speckle size measurement. *Experimental Techniques*, *38*(6), 1–2. doi: 10.1111/ext.12110

Reu, P. (2015). All about speckles: Contrast. *Experimental Techniques*, *39*(1), 1–2. doi: 10.1111/EXT.12126

26911299, 2022, 7, Downloaded from https://currentprotocols.onlinelibrary.wiley.com/doi/10.1002/cpz1.493 by University of Wisconsin,Madison Cam Department of Pathology and, Wiley Online Library on [19/12/2022]. See the Terms and Conditions (https://onlinelibrary.wiley.com/terms-and-conditions) on Wiley Online Library for rules of use; OA articles are governed by the applicable Creative Commons License

Rivlin, R. S. (1948). Large elastic deformations of isotropic materials IV. further developments of the general theory. *Philosophical Transactions of the Royal Society of London. Series A, Mathematical and Physical Sciences*, *241*(835), 379–397. doi: 10.1098/RSTA.1948.0024

Rivlin, R. S., & Saunders, D. W. (1951). Large elastic deformations of isotropic materials VII. Experiments on the deformation of rubber. *Philosophical Transactions of the Royal Society of London. Series A, Mathematical and Physical Sciences*, *243*(865), 251–288. doi: 10.1098/rsta.1951.0004

Sacks, M. S. (1999). A method for planar biaxial mechanical testing that includes in-plane shear. *Journal of Biomechanical Engineering*, *121*(5), 551–555. doi: 10.1115/1.2835086

Sacks, M. S., & Chuong, C. J. (1993). Biaxial mechanical properties of passive right ventricular free wall myocardium. *Journal of Biomechanical Engineering*, *115*(2), 202–205. doi: 10.1115/1.2894122

Sacks, M. S. (2000). Biaxial mechanical evaluation of planar biological materials. *Journal of Elasticity and the Physical Science of Solids*, *61*(1), 199–246. doi: 10.1023/A:1010917028671

Schneider, D. C., Davidson, T. M., & Nahum, A. M. (1984). In vitro biaxial stress-strain response of human skin. *Archives of Otolaryngology*, *110*(5), 329–333. doi: 10.1001/archotol.1984.00800310053012

Seshaiyer, P., & Humphrey, J. D. (2003). A subdomain inverse finite element characterization of hyperelastic membranes including soft tissues. *Journal of Biomechanical Engineering*, *125*(3), 363–371. doi: 10.1115/1.1574333

Shih, E. D., Provenzano, P. P., Witzenburg, C. M., Barocas, V. H., Grande, A. W., & Alford, P. W. (2021). Characterizing tissue remodeling and mechanical heterogeneity in cerebral aneursysms. *Journal of Vascular Research*, *59*, 34–42. doi: 10.1159/000519694

Solav, D., Moerman, K. M., Jaeger, A. M., Genovese, K., & Herr, H. M. (2018). MultiDIC: An open-source toolbox for multi-view 3D digital image correlation. *IEEE Access*, *6*, 30520–30535. doi: 10.1109/ACCESS.2018.2843725

Stella, J. A., & Sacks, M. S. (2007). On the biaxial mechanical properties of the layers of the aortic valve leaflet. *Journal of Biomechanical Engineering*, *129*(5), 757–766. doi: 10.1115/1.2768111

Sun, W., Sacks, M. S., & Scott, M. J. (2005). Effects of boundary conditions on the estimation of the planar biaxial mechanical properties of soft tissues. *Journal of Biomechanical Engineering*, *127*(4), 709–715. doi: 10.1115/1.1933931

Sutton, M., Wolters, W., Peters, W., Ranson, W., & McNeill, S. (1983). Determination of displacements using an improved digital correlation method. *Image and Vision Computing*, *1*(3), 133–139. doi: 10.1016/0262-8856(83)90064-1

Sverdlik, A., & Lanir, Y. (2002). Time-dependent mechanical behavior of sheep digital tendons, including the effects of preconditioning. *Journal of Biomechanical Engineering*, *124*(1), 78–84. doi: 10.1115/1.1427699

Tanaka, Y., Yang, J. M., Liu, Y. F., & Kagawa, Y. (2007). Characterization of nanoscale deformation in a discontinuously reinforced titanium composite using AFM and nanolithography. *Scripta Materialia*, *56*(3), 209–212. doi: 10.1016/J.SCRIPTAMAT.2006.10.015

Thomopoulos, S., Fomovsky, G. M., & Holmes, J. W. (2005). The development of structural and mechanical anisotropy in fibroblast populated collagen gels. *Journal of Biomechanical Engineering*, *127*(5), 742–750. doi: 10.1115/1.1992525

Tong, P., & Fung, Y. C. (1976). The stress-strain relationship for the skin. *Journal of Biomechanics*, *9*(10), 649–657. doi: 10.1016/0021-9290(76)90107-X

Treloar, L. R. G. (1948). Stresses and Birefringence in Rubber subjected to General Homogeneous Strain. *Proceedings of the Physical Society (1926-1948)*, *60*(2), 135. doi: 10.1088/0959-5309/60/2/303

Ventsel, E., & Krauthammer, T. (2001). Thin plates and shells. In *Thin plates and shells*. CRC Press. doi: 10.1201/9780203908723

Walsh, D. R., Lynch, J. J., Connor, O'. D. T., Newport, D. T., & Mulvihill, J. J. E. (2020). Mechanical and structural characterisation of the dural venous sinuses. *Scientific Reports*, *10*(1), 21763. doi: 10.1038/s41598-020-78694-4

Wang, H., Xie, H., Li, Y., & Zhu, J. (2012). Fabrication of micro-scale speckle pattern and its applications for deformation measurement. *Measurement Science and Technology*, *23*(3), 035402. doi: 10.1088/0957-0233/23/3/035402

Weizsäcker, H. W., Lambert, H., & Pascale, K. (1983). Analysis of the passive mechanical properties of rat carotid arteries. *Journal of Biomechanics*, *16*(9), 703–715. doi: 10.1016/0021-9290(83)90080-5

Witzenburg, C., Raghupathy, R., Kren, S. M., Taylor, D. A., & Barocas, V. H. (2012). Mechanical changes in the rat right ventricle with decellularization. *Journal of Biomechanics*, *45*(5), 842–849. doi: 10.1016/j.jbiomech.2011.11.025

Yang, J., & Bhattacharya, K. (2019a). Augmented Lagrangian digital image correlation. *Experimental Mechanics*, *59*(2), 187–205. doi: 10.1007/s11340-018-00457-0

Yang, J., & Bhattacharya, K. (2019b). Fast adaptive global digital image correlation. *Conference Proceedings of the Society for Experimental Mechanics Series*, *12*, 69–73. doi: 10.1007/978-3-319-97481-1_7

Yang, J., Tao, J. L., & Franck, C. (2021). Smart digital image correlation patterns via 3D printing. *Experimental Mechanics*, *61*(7), 1181–1191. doi: 10.1007/S11340-021-00720-X/TABLES/3

Yin, F., Strumpf, R., Chew, P., & Zeger, S. (1987). Quantification of the mechanical properties of noncontracting canine myocardium under simultaneous biaxial loading. *Journal of*

26911299, 2022, 7, Downloaded from https://currentprotocols.onlinelibrary.wiley.com/doi/10.1002/cpz1.493 by University of Wisconsin,Madison Cam Department of Pathology and, Wiley Online Library on [19/12/2022]. See the Terms and Conditions (https://onlinelibrary.wiley.com/terms-and-conditions) on Wiley Online Library for rules of use; OA articles are governed by the applicable Creative Commons License

Biomechanics, *20*(6), 577–589. doi: 10.1016/0021-9290(87)90279-X

Zeng, Y. J., Liu, Y. H., Xu, C. Q., Xu, X. H., Xu, H., & Sun, G. C. (2004). Biomechanical properties of skin in vitro for different expansion methods. *Clinical Biomechanics*, *19*(8), 853–857. doi: 10.1016/J.CLINBIOMECH.2004.05.009

Zhao, X., Chen, X., & Lu, J. (2009). Pointwise identification of elastic properties in nonlinear hyperelastic membranes-part II: Experimental validation. *Journal of Applied Mechanics, Transactions ASME*, *76*(6), 1–8. doi: 10.1115/1.3130810/469751

Zhao, X., Raghavan, M. L., & Lu, J. (2011). Identifying heterogeneous anisotropic properties in cerebral aneurysms: A pointwise approach. *Biomechanics and Modeling in Mechanobiology*, *10*(2), 177. doi: 10.1007/S10237-010-0225-7

Zhou, B., Ravindran, S., Ferdous, J., Kidane, A., Sutton, M. A., & Shazly, T. (2016). Using digital image correlation to characterize local strains on vascular tissue specimens. *Journal of Visualized Experiments*, *2016*(107), 53625. doi: 10.3791/53625

Zhu, R., Xie, H., Xue, Y., Wang, L., & Li, Y. (2015). Fabrication of speckle patterns by focused ion beam deposition and its application to micro-scale residual stress measurement. *Measurement Science and Technology*, *26*(9), 095601. doi: 10.1088/0957-0233/26/9/095601

26911299, 2022, 7, Downloaded from https://currentprotocols.onlinelibrary.wiley.com/doi/10.1002/cpz1.493 by University of Wisconsin,Madison Cam Department of Pathology and, Wiley Online Library on [19/12/2022]. See the Terms and Conditions (https://onlinelibrary.wiley.com/terms-and-conditions) on Wiley Online Library for rules of use; OA articles are governed by the applicable Creative Commons License